

# Intensity dependence of superradiant emission from radiatively coupled excitons in multiple-quantum-well Bragg structures

S. Haas and T. Stroucken

*Department of Physics and Material Sciences Center, Philipps University, Renthof 5, D-35032 Marburg, Germany*

M. Hübner and J. Kuhl

*Max-Planck-Institut für Festkörperforschung, Heisenbergstraße 1, D-70569 Stuttgart, Germany*

B. Grote, A. Knorr, F. Jahnke, and S. W. Koch

*Department of Physics and Material Sciences Center, Philipps University, Renthof 5, D-35032 Marburg, Germany*

R. Hey and K. Ploog

*Paul-Drude-Institut für Festkörperelektronik, Hausvogteiplatz 5-7, D-10177 Berlin, Germany*

(Received 11 July 1997)

Linear time-resolved reflection on the heavy-hole exciton transition of high-quality multiple GaAs quantum-well Bragg samples reveals enhanced radiative emission and accelerated decay of the coherent optical polarization due to radiative interwell coupling. It is shown that this superradiant mode gradually vanishes with increasing excitation intensity. Microscopic calculations attribute this decoupling to the carrier-carrier Coulomb interaction in the individual quantum wells leading to excitation-induced dephasing. The intricate density dependence is discussed comparing computed results for the excitation-dependent decay in single quantum wells and multiple-quantum-well Bragg structures. [S0163-1829(98)02923-3]

## I. INTRODUCTION

Recently, it could be shown that the dynamics of optical excitations in semiconductor multiple-quantum-well (MQW) structures differs considerably from the dynamics in a nominally identical single quantum well (QW).<sup>1-3</sup> The origin for this difference lies in the nature of the radiative decay channel that exists in a composite structure of reduced effective dimensionality. Whereas direct radiative decay of an exciton polariton in a bulk semiconductor is inhibited by the requirement of momentum conservation, a QW exciton with an in-plane momentum  $\hbar k_{\parallel} < \hbar \omega / c$ , where  $\hbar \omega$  is the excitation energy, can decay into a photonic state due to the lack of translational invariance in the growth direction of the structure. Values of the radiative lifetime in the range of a few ps have been postulated theoretically<sup>1,2,4,5</sup> and could be observed experimentally only recently.<sup>3,6,7</sup> Since the field that is emitted by a QW can subsequently interact with other QW's in the sample, the short radiative lifetime of the exciton causes an efficient radiative coupling of the QW's that leads to collective effects. The dynamics of the collective excitations depends strongly on the number of QW's  $N$  and the interwell separation  $d$ . A special situation arises in a MQW Bragg structure, where the interwell spacing  $d$  equals an integer multiple of half the exciton wavelength in the medium  $\lambda_{\text{hh}}$ . At low excitation intensities, the dominant coupling mechanism is a stimulated polarization decay due to reemitted photons. This type of coupling creates a so-called superradiant mode, which ideally is characterized by an  $N$  times enhanced radiative decay rate. The remaining  $N - 1$  "dark" modes then have a vanishing radiative coupling strength.

According to theoretical predictions,<sup>2</sup> the formation of a

superradiant state in a MQW Bragg structure depends critically on the phase matching between optical excitations in different QW's. Therefore, the dynamics of the optical polarization is extremely sensitive to various dephasing mechanisms like scattering at impurities or phonons, interface roughness or excitation-induced dephasing.<sup>8</sup> Moreover, since the concept of superradiance is based on the existence of (quasi)stationary coupled exciton-photon modes, the superradiant mode cannot be an eigenstate of the nonequilibrium coupled semiconductor-photon system at higher excitation intensities.

In this paper, we present theoretical and experimental investigations on the influence of elevated excitation intensities on the dynamics and the formation of the superradiant mode in a MQW Bragg structure. Since an efficient radiative coupling requires phase coherence, only experiments able to identify those photons that are reemitted from the coherent polarization are suited to the study of superradiance. In the coherent regime, the reemission of photons is restricted to the direction of the transmitted and reflected excitation beam by the in-plane momentum conservation. Therefore, we present in this paper experimental and theoretical investigations of the time-resolved reflected signal that directly reveal the enhanced photon emission and the accelerated radiative decay of the coherent polarization. Comparing results of a high-quality GaAs MQW Bragg sample to those of a single QW, the significant reduction of the radiative lifetime can be shown to result from the strong coupling of excitons with phase-coherent photons leading to a stimulated superradiant decay of the excitonic polarization. Similar changes of the exciton lifetime have been observed for QW's located inside microcavities<sup>9,10</sup> or excitons irradiated by phase-controlled coherent optical pulse trains.<sup>11</sup>

The experimental results are analyzed using a microscopic many-body theory that fully includes the radiative coupling of the QW's. Details of that theory and numerical results are described in the following Secs. II and III, respectively. In Sec. IV we present the experimental results and a comparison with theory. Section V gives a brief summary and conclusion and in the Appendix we generalize the analysis of Ref. 2 to compute the quasistationary coupled exciton-photon modes of the semiconductor Maxwell-Bloch equations.

## II. THEORETICAL MODEL

The propagation of a classical light pulse  $\mathbf{E}$  in a semiconductor structure is described by the wave equation

$$[\Delta - 1/c^2 \partial_t^2] \mathbf{E}(\mathbf{r}, t) = 4\pi/c_v^2 \partial_t^2 \mathbf{P}(\mathbf{r}, t) - 4\pi \nabla \nabla \cdot \mathbf{P}(\mathbf{r}, t), \quad (1)$$

where  $c_v$  is the vacuum light velocity,  $c = c_v/\sqrt{\epsilon}$  is the speed of light in the sample,  $\epsilon$  is the background dielectric constant, and  $\mathbf{P}$  is the resonant contribution to the total polarization in the QW's. Restricting our analysis to pulse propagation perpendicular to the QW planes, applying the boundary conditions at the interfaces between QW and barrier material, and using an envelope function approximation for the  $z$  dependence of  $\mathbf{P}$  we obtain for each circular polarization component of the electromagnetic field within the semiconductor structure<sup>2</sup>

$$E(z, t) = E_1^+(t - z/c) - \frac{2\pi}{c\epsilon_{n=1}} \sum_{n=1}^N \partial_t P_n(t - |z - z_n|/c). \quad (2)$$

Here,  $z_n$  is the position and  $P_n$  the polarization of the  $n$ th QW.  $E_1^+$  denotes that part of the optical field in the first barrier that propagates in the positive  $z$  direction.

In order to allow for a realistic comparison of the computed results with experimental observations we include in the following, in addition to the analysis in Ref. 2, also reflections at the sample surface whereas we assume the substrate to be absorbing. From Maxwell's equations one can construct the boundary conditions for the vacuum/semiconductor interface:

$$E_0(t) + E_R(t) = E_1^+(t) + E_1^-(t), \quad (3a)$$

$$E_0(t) - E_R(t) = \sqrt{\epsilon}(E_1^+(t) - E_1^-(t)). \quad (3b)$$

Here, we denote the input field as  $E_0$ , the total reflected field as  $E_R$  and the forward and backward propagating fields in the first barrier as  $E_1^+$  and  $E_1^-$ , respectively. Combining Eqs. (2) and (3), we obtain

$$E(z, t) = \frac{2}{\sqrt{\epsilon+1}} E_0(t - z/c) - \frac{2\pi}{c\epsilon_{n=1}} \sum_{n=1}^N \partial_t P_n(t - |z - z_n|/c) - \frac{\sqrt{\epsilon-1}}{\sqrt{\epsilon+1}} \frac{2\pi}{c\epsilon_{n=1}} \sum_{n=1}^N \partial_t P_n(t - (z + z_n)/c), \quad z > 0 \quad (4)$$

for the electromagnetic field inside the structure. The total reflected field outside the sample is given by

$$E_R(z, t) = -\frac{\sqrt{\epsilon-1}}{\sqrt{\epsilon+1}} E_0(t + z/c_v) - \frac{2\sqrt{\epsilon}}{\sqrt{\epsilon+1}} \frac{2\pi}{c\epsilon_{n=1}} \sum_{n=1}^N \partial_t P_n(t - z_n/c + z/c_v), \quad z < 0. \quad (5)$$

The first term on the right hand side of Eq. (4) is the incident laser field transmitted at the vacuum/semiconductor interface, the second term represents the fields emitted from the  $n$ th QW at position  $z_n$ , and the last term results from the internal reflection of the emitted fields at the sample surface. Clearly, the dynamics of the coupled exciton-photon modes is modified by the cladding layers due to these internal reflections at the sample/air interface. In the results, these modifications can either lead to an apparent enhancement or reduction of the radiative coupling, depending on the thickness of the first barrier (see Fig. 8 and Appendix for further details).

To solve Eqs. (4) and (5), the polarization  $P_n$  within the  $n$ th QW must be calculated from a microscopic model. For this purpose, we start from the standard two-band Hamiltonian including the free motion of the carriers in a confinement potential superposed on the periodic lattice potential, the Coulomb interaction between carriers and the dipole interaction between carriers and light field.<sup>12</sup> To take into account the confinement of the QW electrons in  $z$  direction, the Bloch wave functions are expanded into plane waves for the in-plane coordinates and the envelope functions perpendicular to the QW for the first electron and hole subband only. Expanding the macroscopic polarization of QW  $n$  in the one-particle momentum states, we have  $P_n(t) = 1/A \sum_{\mathbf{k}} \mu_{\mathbf{k}} p_{\mathbf{k},n}(t)$  where  $\mu_{\mathbf{k}}$  is the dipole matrix element between valence and conduction band and  $A$  is the normalization area. Within this basis the equations of motion for the coherent interband polarization  $p_{\mathbf{k},n}$  and the carrier occupation probability  $f_{\mathbf{k},n}^{e/h}$  are derived using Green's function techniques.<sup>13</sup> Restricting our analysis to contributions up to second order in the Coulomb potential, we obtain in second Born approximation for the polarization and population distributions in the  $n$ th QW:<sup>14</sup>

$$[i\hbar \partial_t - \epsilon_{\mathbf{k},n}^e(t) - \epsilon_{\mathbf{k},n}^h(t) + i\hbar \gamma_0] p_{\mathbf{k},n}(t) + [1 - f_{\mathbf{k},n}^e(t) - f_{\mathbf{k},n}^h(t)] \Omega_{\mathbf{k},n}(t) = i[-S_{\mathbf{k},n}^D(t) + S_{\mathbf{k},n}^{OD}(t) + V_{\mathbf{k},n}^D(t) - V_{\mathbf{k},n}^{OD}(t)], \quad (6)$$

$$i\hbar \partial_t f_{\mathbf{k},n}^{e/h}(t) + \Omega_{\mathbf{k},n}(t) p_{\mathbf{k},n}^*(t) - \Omega_{\mathbf{k},n}^*(t) p_{\mathbf{k},n}(t) = i[s_{\mathbf{k},n}^f(t) + s_{\mathbf{k},n}^D(t) + s_{\mathbf{k},n}^{OD}(t) + v_{\mathbf{k},n}^D(t) - v_{\mathbf{k},n}^{OD}(t)]. \quad (7)$$

Here we added a small phenomenological background dephasing  $\gamma_0$ , representing contributions due to interactions of coherent excitons with sample imperfections (defects, interface roughness, alloy fluctuations in the barriers, etc.) or phonons. The left hand sides of Eqs. (6) and (7) contain the Hartree-Fock renormalizations

$$\varepsilon_{\mathbf{k},n}^{e/h}(t) = \varepsilon_{\mathbf{k}}^{e/h} - \frac{1}{A} \sum_{\mathbf{k}'} V_{\mathbf{k}-\mathbf{k}'} f_{\mathbf{k}',n}^{e/h}(t), \quad (8)$$

$$\Omega_{\mathbf{k},n}(t) = \mu_{\mathbf{k}} E(z_n, t) + \frac{1}{A} \sum_{\mathbf{k}'} V_{\mathbf{k}-\mathbf{k}'} p_{\mathbf{k}',n}(t), \quad (9)$$

where  $V$  is the bare quasi-two-dimensional Coulomb potential and  $\varepsilon_{\mathbf{k}}^{e/h} = \hbar^2 k^2 / 2m_{e/h}$  is the free particle energy of an electron/hole in state  $\mathbf{k}$ . In the following, we suppress the QW subscript  $n$  and the time argument  $t$  for better readability. The right hand side of Eq. (6) contains the dephasing processes due to the Coulomb interaction, which are divided into diagonal (D) and off-diagonal (OD) contributions:

$$S_{\mathbf{k}}^D = \frac{1}{A^2} \sum_{\mathbf{k}', \mathbf{k}''} \sum_{a,b=e,h} g(\varepsilon_{\mathbf{k}}^a + \varepsilon_{\mathbf{k}'+\mathbf{k}''}^b - \varepsilon_{\mathbf{k}''}^b - \varepsilon_{\mathbf{k}'+\mathbf{k}}^a) \times [2W_{\mathbf{k}'}^2 - \delta_{ab} W_{\mathbf{k}'} W_{\mathbf{k}-\mathbf{k}''}] p_{\mathbf{k}} [(1-f_{\mathbf{k}'+\mathbf{k}''}^b) f_{\mathbf{k}''}^b f_{\mathbf{k}'+\mathbf{k}}^a + f_{\mathbf{k}'+\mathbf{k}''}^b (1-f_{\mathbf{k}''}^b) (1-f_{\mathbf{k}'+\mathbf{k}}^a) - p_{\mathbf{k}'+\mathbf{k}''}^* p_{\mathbf{k}}^*], \quad (10)$$

$$S_{\mathbf{k}}^{OD} = \frac{1}{A^2} \sum_{\mathbf{k}', \mathbf{k}''} \sum_{a,b=e,h} g(-\varepsilon_{\mathbf{k}}^a - \varepsilon_{\mathbf{k}'+\mathbf{k}''}^b + \varepsilon_{\mathbf{k}''}^b + \varepsilon_{\mathbf{k}'+\mathbf{k}}^a)$$

$$\times [2W_{\mathbf{k}'}^2 - \delta_{ab} W_{\mathbf{k}'} W_{\mathbf{k}-\mathbf{k}''}] p_{\mathbf{k}'+\mathbf{k}} [(1-f_{\mathbf{k}}^a) \times (1-f_{\mathbf{k}'+\mathbf{k}''}^b) f_{\mathbf{k}''}^b + f_{\mathbf{k}'}^a f_{\mathbf{k}'+\mathbf{k}''}^b (1-f_{\mathbf{k}}^b) - p_{\mathbf{k}'+\mathbf{k}''}^* p_{\mathbf{k}}^*], \quad (11)$$

$$V_{\mathbf{k}}^D = \frac{1}{A^2} \sum_{\mathbf{k}', \mathbf{k}''} \sum_{a=e,h} g(\varepsilon_{\mathbf{k}}^a - \varepsilon_{\mathbf{k}'+\mathbf{k}''}^{\bar{a}} + \varepsilon_{\mathbf{k}''}^{\bar{a}} - \varepsilon_{\mathbf{k}'+\mathbf{k}}^a) \times W_{\mathbf{k}'} W_{\mathbf{k}-\mathbf{k}''} p_{\mathbf{k}} [p_{\mathbf{k}'+\mathbf{k}}^* - p_{\mathbf{k}'+\mathbf{k}''}^*] p_{\mathbf{k}}^*, \quad (12)$$

$$V_{\mathbf{k}}^{OD} = \frac{1}{A^2} \sum_{\mathbf{k}', \mathbf{k}''} \sum_{a=e,h} g(-\varepsilon_{\mathbf{k}}^a + \varepsilon_{\mathbf{k}'+\mathbf{k}''}^{\bar{a}} - \varepsilon_{\mathbf{k}''}^{\bar{a}} + \varepsilon_{\mathbf{k}'+\mathbf{k}}^a) \times W_{\mathbf{k}'} W_{\mathbf{k}-\mathbf{k}''} \{ p_{\mathbf{k}'+\mathbf{k}} [(1-f_{\mathbf{k}}^a) f_{\mathbf{k}'+\mathbf{k}''}^{\bar{a}} (1-f_{\mathbf{k}''}^{\bar{a}}) + f_{\mathbf{k}}^a (1-f_{\mathbf{k}'+\mathbf{k}''}^{\bar{a}}) f_{\mathbf{k}''}^{\bar{a}}] - p_{\mathbf{k}'+\mathbf{k}''} [(1-f_{\mathbf{k}}^a) (1-f_{\mathbf{k}''}^{\bar{a}}) f_{\mathbf{k}'+\mathbf{k}}^a + f_{\mathbf{k}}^a f_{\mathbf{k}''}^{\bar{a}} (1-f_{\mathbf{k}'+\mathbf{k}}^a)] \}. \quad (13)$$

Here,  $W$  denotes the screened Coulomb potential,  $g(x) = \pi \delta(x) + iP/x$  and  $\bar{a} = h(e)$  for  $a = e(h)$ , respectively. For the electron ( $a = e$ ) and hole ( $a = h$ ) distribution functions the relaxation contributions in Eq. (7) are

$$s_{\mathbf{k}}^f = \frac{2\pi}{A^2} \sum_{\mathbf{k}', \mathbf{k}''} \sum_{b=e,h} \delta(\varepsilon_{\mathbf{k}}^a + \varepsilon_{\mathbf{k}'+\mathbf{k}''}^b - \varepsilon_{\mathbf{k}''}^b - \varepsilon_{\mathbf{k}'+\mathbf{k}}^a) [2W_{\mathbf{k}'}^2 - \delta_{ab} W_{\mathbf{k}'} W_{\mathbf{k}-\mathbf{k}''}] [(1-f_{\mathbf{k}}^a) (1-f_{\mathbf{k}'+\mathbf{k}''}^b) f_{\mathbf{k}''}^b f_{\mathbf{k}'+\mathbf{k}}^a - f_{\mathbf{k}}^a f_{\mathbf{k}'+\mathbf{k}''}^b (1-f_{\mathbf{k}''}^b) (1-f_{\mathbf{k}'+\mathbf{k}}^a)], \quad (14)$$

$$s_{\mathbf{k}}^{OD} = \frac{1}{A^2} \sum_{\mathbf{k}', \mathbf{k}''} \sum_{b=e,h} g(\varepsilon_{\mathbf{k}}^a + \varepsilon_{\mathbf{k}'+\mathbf{k}''}^b - \varepsilon_{\mathbf{k}''}^b - \varepsilon_{\mathbf{k}'+\mathbf{k}}^a) [2W_{\mathbf{k}'}^2 - \delta_{ab} W_{\mathbf{k}'} W_{\mathbf{k}-\mathbf{k}''}] [f_{\mathbf{k}}^a - f_{\mathbf{k}'+\mathbf{k}}^a] p_{\mathbf{k}'+\mathbf{k}''}^* p_{\mathbf{k}}^* + \text{c.c.}, \quad (15)$$

$$s_{\mathbf{k}}^D = \frac{1}{A^2} \sum_{\mathbf{k}', \mathbf{k}''} \sum_{b=e,h} g(\varepsilon_{\mathbf{k}}^{\bar{a}} + \varepsilon_{\mathbf{k}'+\mathbf{k}''}^b - \varepsilon_{\mathbf{k}''}^b - \varepsilon_{\mathbf{k}'+\mathbf{k}}^{\bar{a}}) [2W_{\mathbf{k}'}^2 - \delta_{\bar{a}b} W_{\mathbf{k}'} W_{\mathbf{k}-\mathbf{k}''}] [f_{\mathbf{k}''}^b - f_{\mathbf{k}'+\mathbf{k}''}^b] p_{\mathbf{k}} p_{\mathbf{k}'+\mathbf{k}}^* + \text{c.c.}, \quad (16)$$

$$v_{\mathbf{k}}^{OD} = \frac{-1}{A^2} \sum_{\mathbf{k}', \mathbf{k}''} g(-\varepsilon_{\mathbf{k}}^a + \varepsilon_{\mathbf{k}'+\mathbf{k}''}^{\bar{a}} - \varepsilon_{\mathbf{k}''}^{\bar{a}} + \varepsilon_{\mathbf{k}'+\mathbf{k}}^a) W_{\mathbf{k}'} W_{\mathbf{k}-\mathbf{k}''} \{ [f_{\mathbf{k}}^a - f_{\mathbf{k}'+\mathbf{k}}^a] p_{\mathbf{k}'+\mathbf{k}''}^* p_{\mathbf{k}}^* - [f_{\mathbf{k}}^a - f_{\mathbf{k}'+\mathbf{k}}^{\bar{a}}] p_{\mathbf{k}'+\mathbf{k}}^* p_{\mathbf{k}}^* \} + \text{c.c.}, \quad (17)$$

$$v_{\mathbf{k}}^D = \frac{1}{A^2} \sum_{\mathbf{k}', \mathbf{k}''} g(\varepsilon_{\mathbf{k}}^{\bar{a}} - \varepsilon_{\mathbf{k}'+\mathbf{k}''}^a + \varepsilon_{\mathbf{k}''}^a - \varepsilon_{\mathbf{k}'+\mathbf{k}}^{\bar{a}}) W_{\mathbf{k}'} W_{\mathbf{k}-\mathbf{k}''} \{ [f_{\mathbf{k}''}^a - f_{\mathbf{k}'+\mathbf{k}''}^a] p_{\mathbf{k}} p_{\mathbf{k}'+\mathbf{k}}^* - [f_{\mathbf{k}''}^a - f_{\mathbf{k}'+\mathbf{k}}^{\bar{a}}] p_{\mathbf{k}} p_{\mathbf{k}'+\mathbf{k}}^* \} + \text{c.c.} \quad (18)$$

Equations (4), (6), and (7) constitute the semiconductor Maxwell-Bloch equations (SMBE's). The SMBE's take into account light propagation effects such as absorption and re-emission of photons by the coherently polarized exciton transition. In the linear or quasistationary regime, the solutions can be expressed in terms of stationary coupled exciton-photon (polariton) modes, which have well-defined energies and radiative linewidths. A detailed analysis of the quasistationary modes is given in the Appendix.

The solution of the SMBE's in the form presented above constitutes a rather challenging numerical problem. Due to the various summations in the scattering rates, the evaluation

of the dephasing and relaxation contributions for each  $\mathbf{k}$  point, especially, is extremely CPU time consuming. To deal with this problem we have evaluated the rates  $S_{k_i}, V_{k_i}, s_{k_i}, v_{k_i}$ ,  $i = 1, \dots, n_k$  using massively parallel numerical schemes.

### III. NUMERICAL RESULTS AND DISCUSSION

As examples of the numerical results we discuss in the following the computed time-dependent reflection for a SQW and a perfect  $N=10$  Bragg structure assuming 80-Å GaAs QW's and a top layer of 45-nm AlGaAs.<sup>15</sup> This QW

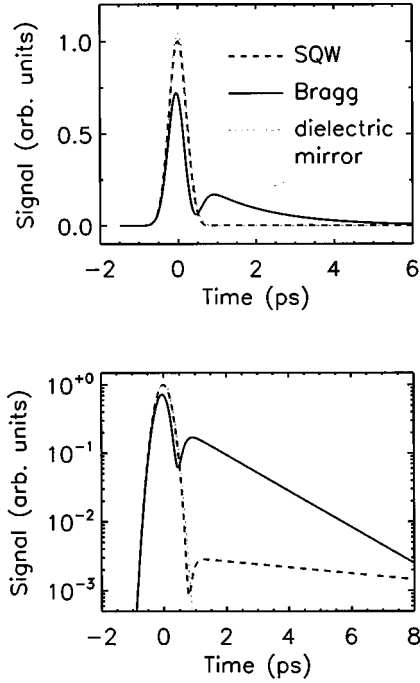


FIG. 1. Calculated linear reflection of laser pulses resonant to the heavy-hole exciton from a perfect  $N=10$  Bragg structure (solid line), and from a single quantum well (dashed line) on a linear (upper) and logarithmic scale (lower part). For reference the reflected laser pulse at a dielectric mirror with the same dielectric constant as the barrier material is shown (dotted line).

thickness is small enough to make it possible to neglect contributions from the light-hole exciton transition.

Figure 1 shows the results for low excitation intensities on a linear (upper) and logarithmic scale (lower part). Here, resonant excitation of the hh-exciton transition with a Gaussian pulse of 530-fs full width at half-maximum (FWHM) is assumed. The signal intensity has been normalized to the maximum intensity reflected from the SQW, that occurs at  $t=0$ . As reference the direct reflection of the incident pulse is shown, which would be found when the sample is replaced by a dielectric mirror with the same dielectric constant as the barrier material. Of special importance are those parts of the reflected signal that are seen for times at which the direct reflection of the incident pulse has decayed. These components result from reemission of light that is transiently absorbed by the quantum well(s). The signal from the Bragg structure shows a double peak signature as a function of time resulting from the destructive interference between the directly reflected signal and the signal coherently emitted from the quantum wells. For a pulse duration of 530 fs (FWHM) the signal intensity reaches its maximum approximately 1 ps after the arrival of the pulse maximum. At later times the signals reveal a single exponential decay resulting from the radiative decay of the excitation in the QW's. Under the conditions chosen for the calculations, this decay is dominated by the optical dephasing of the coherent polarization of the lowest exciton transition. In real samples, inhomogeneous broadening of the excitonic resonances may provide further contributions to the signal decay, depending on the amount of energetic disorder in the sample.

The dephasing rate comprises radiative and nonradiative

(denoted by  $\Gamma$  and  $\gamma_0$ , respectively) contributions. In the linear regime, the radiative dephasing rate of the two-dimensional (2D) exciton in the absence of the cladding layers can be calculated from the dipole matrix element  $\mu_{\mathbf{k}}$ , the wavelength in the medium corresponding to the excitonic transition  $\lambda_{hh}$  and the overlap of the electron-hole wave functions according to  $\Gamma = 4\pi^2 |\sum_{\mathbf{k}} \mu_{\mathbf{k}} \varphi(\mathbf{k})|^2 / \epsilon \lambda_{hh}$ , which depends on the QW thickness through the excitonic wave function  $\varphi(\mathbf{k})$ . Including reflections at the vacuum/semiconductor interface, the radiative dephasing rate of a SQW is given by

$$\Gamma_s = \Gamma \left( 1 + \frac{\sqrt{\epsilon} - 1}{\sqrt{\epsilon} + 1} \cos(4\pi d_1 / \lambda_{hh}) \right), \quad (19)$$

where  $d_1$  is the thickness of the first barrier (see Appendix). Using  $1/\Gamma = 17$  ps and  $d_1 = 0.21\lambda_{hh}$  yields a radiative dephasing time  $1/\Gamma_s = 33$  ps. Note that due to the finite well width, the value of  $\Gamma$  used here is smaller than the decay rates of Refs. 2 and 3 which are computed for the ideal 2D limit. Estimating a nonradiative contribution of  $1/\gamma_0 = 50$  ps, we obtain  $T_2 = (\gamma_0 + \Gamma_s)^{-1} = 20$  ps for the SQW and  $T_2 = (\gamma_0 + N\Gamma_s)^{-1} = 3.1$  ps for the  $N=10$  Bragg sample. Thus the theory predicts a pronounced decrease of the signal decay time for the  $N=10$  sample. However, it is important to note that the ideally  $N$  times decreased radiative lifetime in a MQW Bragg structure as compared to a SQW can only be expected if the samples have negligible nonradiative homogeneous and inhomogeneous linewidth *and identical top layers*. However, the quadratic increase of the superradiant emission intensity with  $N$  due to constructive interference of the electric fields reradiated by the excitonic polarization in a Bragg sample is independent of the top layer.

As has been mentioned in the Introduction, the formation of the superradiant mode depends extremely sensitively on phase coherence within the MQW structure. Phase coherence can be destroyed either by deviations (both random and systematic) from the Bragg condition or by intrinsic dephasing mechanisms like scattering at impurities or interface roughness, phonon or Coulomb scattering. Whereas a study of the effects of dephasing due to static disorder requires a whole series of samples, effects of excitation-induced dephasing can be investigated systematically by varying the excitation intensity. Furthermore, it is important to note that there is a fundamental difference between excitation-induced dephasing and dephasing due to static disorder or phonon scattering. Whereas disorder leads to dephasing in the linear regime where the solutions of the SMBE can be expressed in terms of stationary exciton-photon modes, an increase of the excitation intensity requires the solution of the full nonlinear SMBE for the nonequilibrium system where the coupling of the QW's can no longer be described by the formation of (quasi)stationary exciton-photon modes. Thus, the formation of a superradiant state is not only affected by dephasing mechanisms but also by optical nonlinearities like phase space filling, Coulomb screening, etc.

To study the influence of the nonlinear Coulombic effects, we show in Fig. 2 the computed normalized reflected signal of a  $N=10$  MQW Bragg structure for different excitation intensities. The excitation intensity is given in terms of the Rabi energy  $\Omega_R = 2/(\sqrt{\epsilon} + 1) \mu_{\mathbf{k}=0} E_0(t=0)$ , which is a di-

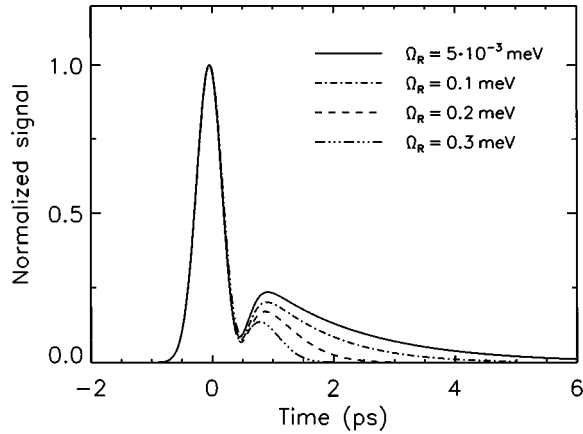


FIG. 2. Calculated reflection of laser pulses resonant to the heavy-hole exciton from a perfect  $N=10$  Bragg structure for different excitation intensities.

rect measure of the excitation intensity within the sample. Figure 2 clearly shows that the second peak in the signal, i.e., that part that originates from the reradiation of the MQW structure, is strongly reduced for increasing excitation intensities. To analyze the origin of these intensity dependent effects we plot in Figs. 3(a) and 3(b) the numerical results for the reflection of a SQW and the Bragg structure under identical excitation conditions on a logarithmic scale. We see that with increasing intensity the total decay rate increases significantly in both structures and simultaneously the maximum of the signal amplitude decreases. The increased decay rate of the reradiated signal is a clear signature of the excitation-induced dephasing resulting from the Coulomb scattering effects in the quantum well(s).

In Fig. 3(c) we plot the ratio of the SQW and Bragg results. Apart from modifications for times less than the laser pulse duration, which can be explained by interference of the QW signal and the initial laser pulse, all signal amplitude ratios start at a value of  $N^2=100$  due to the constructive interference of the signal emitted from different QW's in the Bragg sample. In the linear regime, the ratio decreases with increasing time due to the enhanced radiative decay rate in the Bragg structure. However, at higher excitation levels the decrease of the signal ratio slows down until the total decay rate of the SQW even exceeds that of the Bragg structure such that the signal ratio even increases with increasing time. This surprising result can be understood by noting that the photogenerated carrier density depends on the detailed interplay between radiative and nonradiative decay processes. The fast radiative decay in a MQW Bragg sample prevents the coherent polarization from being efficiently scattered into nonradiative states, i.e., being incoherently absorbed. Thus, the carrier density generated in a MQW Bragg structure can become significantly smaller than the carrier density in a SQW under identical excitation conditions, which is shown in Fig. 4. Hence, for moderate excitations the excitation induced dephasing in the SQW is sufficiently more pronounced than in the Bragg structure for the same excitation intensities. Hence, the total decay rate of the SQW eventually exceeds that of the Bragg structure. It is worth noting that for increasing excitation intensity, the ratio of the generated carrier density in a Bragg structure and a SQW eventually approaches unity. In this limit, the dynamics of the

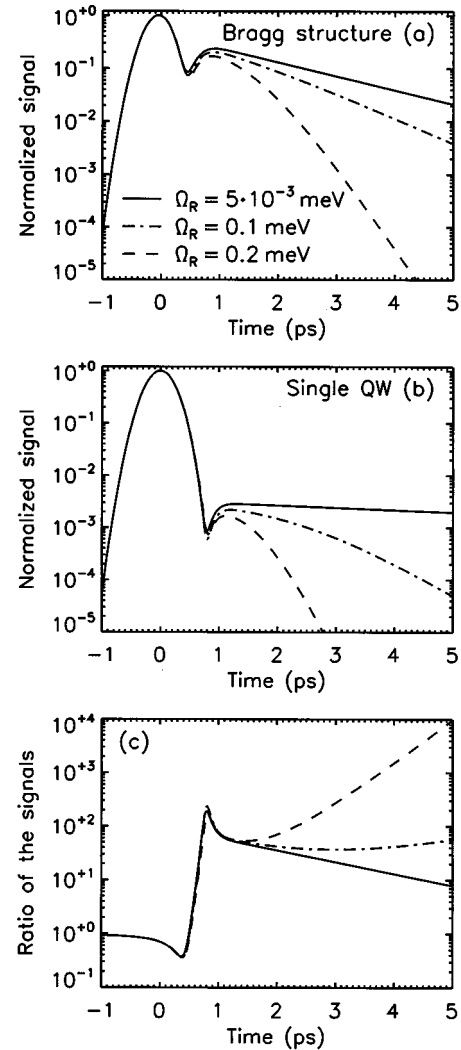


FIG. 3. Comparison of the calculated reflected signals emitted from a  $N=10$  MQW Bragg structure (a) and a SQW (b) for different excitation intensities. In (c) the calculated ratio of the reflected signal from a  $N=10$  MQW Bragg structure and a SQW for various excitation intensities is shown.

reflected signal is dominated completely by the Coulomb scattering, while the radiative coupling is of minor importance.

#### IV. EXPERIMENTAL RESULTS AND DISCUSSION

To study the main effects found in the theoretical analysis we performed experiments on two GaAs/(Al,Ga)As samples grown by molecular-beam epitaxy on semi-insulating GaAs substrates: one SQW and a MQW consisting of  $N=10$  GaAs QW's of 20 nm thickness between  $\text{Al}_{0.3}\text{Ga}_{0.7}\text{As}$  barriers, the thicknesses of which were chosen to satisfy the Bragg condition. The Bragg sample has a 47-nm top layer, while the SQW sample has a 118-nm top layer. The low-temperature photoluminescence linewidth amounts to 0.25 and 0.45 meV for the SQW and the Bragg structure, respectively. All experiments were performed at  $T=8$  K with 100-fs pulses from a Kerr-lens mode-locked Ti:sapphire laser. The laser output was split into two parts. The first pulse is passed through a pulse shaper in order to reduce the spec-

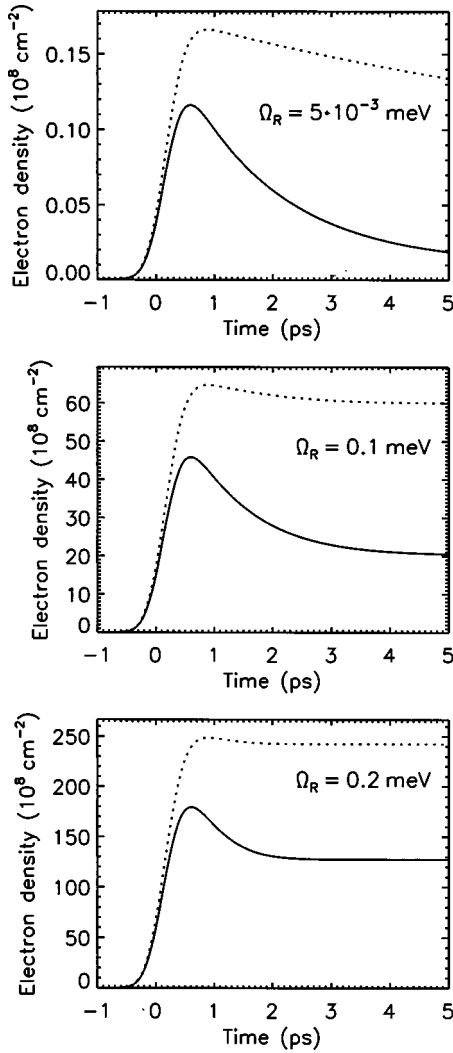


FIG. 4. Calculated photogenerated carrier densities in a SQW (dotted lines) and a  $N=10$  MQW Bragg structure (solid lines) for different excitation intensities.

tral bandwidth to 3.3 meV, thus avoiding band-to-band excitation of free carriers. Behind the pulse shaper the pulse duration amounts to approximately 800 fs. This pulse is used to probe the reflectivity at the hh-exciton transition. The reflected beam is superimposed to the second strong 100-fs pulse in a 2-mm-thick  $\text{LiIO}_3$  crystal for upconversion. The sum frequency signal in dependence on the real-time delay between the reflected pulse and the upconversion pulse provides time resolution of the linear reflection signal.

Figure 5 depicts the measured shapes of the reflected pulse for the SQW and the  $N=10$  MQW Bragg sample measured at a very low average probe pulse intensity of  $2 \text{ W/cm}^2$ . The experimental results agree fairly well with the computed results shown in Fig. 1. The first peak follows the cross correlation trace of the probe with the upconversion pulse and can be attributed to reflection at the sample/air interface. On the trailing edge both signals exhibit the decay of the resonantly excited polarization of the hh-exciton transition in the QW's. This signal part is roughly 100 times higher for the Bragg structure because of the constructive interference of the Bragg-reflected polarization in agreement with the theoretical predictions. However, the relative mag-

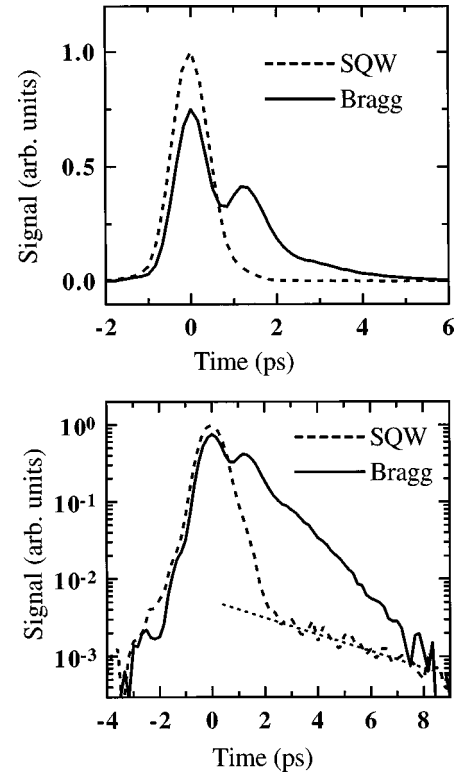


FIG. 5. Comparison of the time-resolved reflected pulses from a  $N=10$  Bragg structure (solid line), and from a single quantum well (dashed line), at low excitation intensity on a linear (upper) and logarithmic scale (lower part).

nitude of the signal emitted from the QW polarization and the signal reflected at the first interface is significantly larger than predicted by our numerical calculations. Furthermore, the observed signal exhibits a two-stage decay in contrast to the theoretical predictions.

The experimentally observed two-stage decay of the signal emitted from the Bragg sample results most likely from imperfect external pulse shaping. To test this assumption we performed calculations using a non-Gaussian exciting laser pulse. As shown in Fig. 6 the computed results mimic the experimental observations. For these calculations we mod-

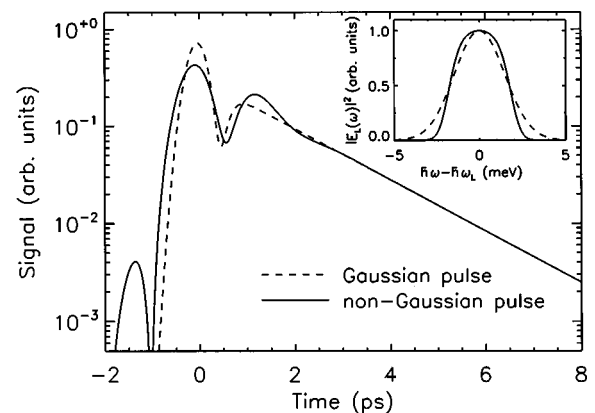


FIG. 6. Calculated linear reflected signal from a  $N=10$  Bragg structure excited with a non-Gaussian laser pulse (solid line) in comparison to excitation with a Gaussian laser pulse of equal FWHM (dashed line).

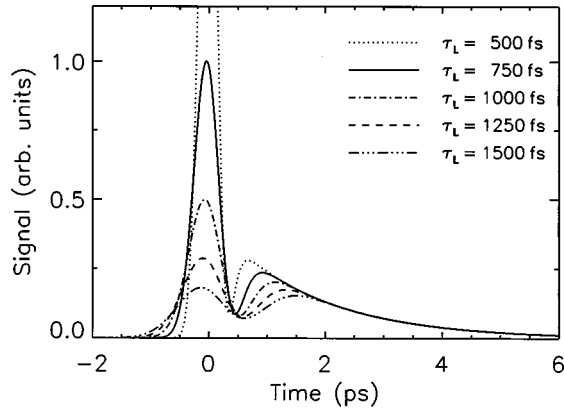


FIG. 7. Calculated dependence of the reflected signal on the laser pulse duration.

eled a pulse shaping in frequency space according to  $E(\omega) = E_0(\omega)f(-\beta(\omega - \omega_L + \Delta\omega))f(\beta(\omega - \omega_L - \Delta\omega))$  where  $E_0$  is a Gaussian of 14 meV FWHM,  $f(x) = [\exp(x) + 1]^{-1}$  is a Fermi function,  $\omega_L$  is the central laser frequency,  $\hbar\Delta\omega = 2.1$  meV, and  $\beta = 1.6$  ps. The calculated signal amplitudes shown in Fig. 6 are normalized with the signal maximum obtained at  $t=0$  from a single quantum well using the Gaussian pulse. Comparison of the signals emitted from the Bragg sample obtained using a non-Gaussian and a Gaussian laser pulse with comparable spectral width shows that the long-time behavior of the signal is not affected by the external pulse shape, whereas on a short-time scale the signal is determined by interference of the MQW signal and the input pulse. In particular, the peak height and the temporal position of the signal maximum depend on the duration of the exciting pulse. This is illustrated in Fig. 7 where the calculated signal from a  $N=10$  Bragg structure is shown for various temporal widths  $\tau_L$  of the exciting pulse. Increasing  $\tau_L$  shifts the second peak to later times, even though for all pulses the time-integrated excitation intensity  $\int dt \mu_{k=0} E_0(t)/\hbar$  has been kept constant. Under these conditions the emitted signal of the MQW Bragg structure does not depend on the laser pulse duration as can be verified from the signal for times larger than  $\tau_L$ . Hence, the signal modifications for times less than  $\tau_L$  are a result of the destructive interference. Furthermore we note that for longer pulses the maximum of the directly reflected part of the signal is reduced compared to the reemitted part.

The experimentally observed single exponential decay of the signals for  $\tau > 2$  ps indicate high sample quality, since an inhomogeneous broadening would result in a nonexponential polarization decay. Also, degenerate four-wave-mixing (DFWM) experiments<sup>3</sup> confirm high sample quality. Linear fits to the experimental curves at long times yield dephasing times  $T_2$  of 7.6 ps and 2.3 ps for the SQW and the  $N=10$  Bragg structure, respectively. Assuming a nonradiative contribution to the dephasing time of  $1/\gamma_0 = 37$  ps, which can be estimated from DFWM experiments, these  $T_2$  times correspond to radiative decay times of 9.6 ps for the SQW and 2.5 ps for the superradiant mode in the Bragg structure. Due to the different top layers in our structures, the enhancement of the radiative decay rate is much smaller than the ideal value of 10. To illustrate the effect of the first top layer on the signal decay, we plotted in Fig. 8 the calculated linear re-

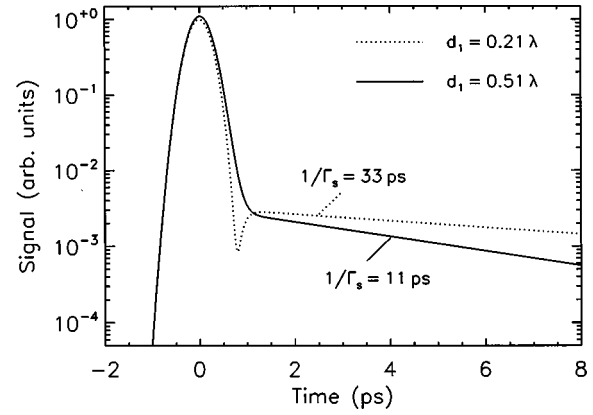


FIG. 8. Dependence of the calculated linear reflected signal from a single quantum well with  $1/\Gamma_s = 17$  ps on the cladding layer.

lected signal of a SQW with an intrinsic radiative dephasing time of 17 ps and a top layer of  $d_1 = 0.51\lambda$ , which roughly corresponds to our 118-nm top layer, and for  $d_1 = 0.21\lambda$ , which has already been shown in Sec. II. Using Eq. (19) the radiative dephasing rate  $\Gamma$  can be estimated from the observed signal decay times in Fig. 5, yielding  $1/\Gamma = 15$  ps for the SQW and  $1/\Gamma = 13$  ps for the Bragg structure. These values agree quite well with each other and with the theoretical prediction.

The value of  $T_2$  for the superradiant mode in the Bragg structure is distinctively smaller than the fast initial decay time observed in time-integrated DFWM experiments.<sup>3</sup> This discrepancy most likely originates from sample disorder such as fluctuations of the QW or barrier widths. As shown in previous papers<sup>2</sup> the presence of disorder implies a certain amount of transfer of oscillator strength to the optically dark modes, which are forbidden in a perfect Bragg sample. The DFWM experiment measures contributions of both the superradiant and the weakly radiant modes whereas the reflected signal is dominated by the superradiant mode.

To study the effects of phase coherence on the formation of the superradiant mode we control the dephasing rate by varying the intensity of the incident laser beam. The density dependence of the time-resolved reflection signal depicted in Fig. 9 demonstrates rapid disappearance of the superradiant emission at higher excitation levels due to rapid phase coherence loss caused by the excitation-induced dephasing within the individual wells.<sup>8</sup> Variation of the average probe power over three orders of magnitude from 5  $\mu$ W to 5 mW results in a complete suppression of the superradiant emission. This is also demonstrated by the inset of Fig. 9, where the area under the normalized curves is plotted against the intensity. The total change of the integrated pulse area for the lowest and highest intensities is about 23%. For the intensities larger than 5 mW the pulse reflected from the Bragg sample has the same shape as the incident pulse observed when the sample was replaced by a gold mirror. The slight modulation of the signal at  $-1$  ps delay in Fig. 9 presumably results from imperfect external pulse shaping.

## V. CONCLUSION

In conclusion, our theoretical investigation of time-resolved reflection experiments on MQW Bragg structures and the corresponding single quantum well clearly shows the

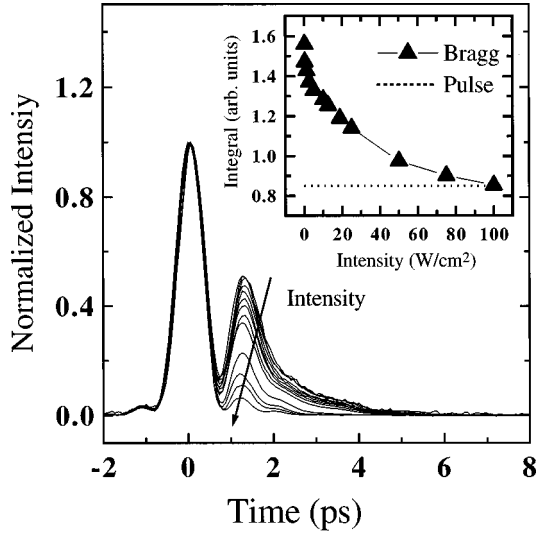


FIG. 9. Normalized reflected signals from the  $N=10$  Bragg structure in dependence on the excitation intensity. Inset: Integral under the normalized curves in dependence on intensity. The formation of the superradiant signal is more and more suppressed with increasing pulse intensity.

superradiant emission from the radiatively coupled excitons under transient resonant excitation. The theoretical analysis reveals an intricate interplay between excitation-induced dephasing and superradiant decay of the excitation in a MQW Bragg structure. Efficient radiative coupling requires phase coherence between the excited excitons. Theory and experiment show a suppression of the superradiant mode for increased excitation intensities due to excitation-induced dephasing.

The experimental results are well reproduced by solutions of the semiconductor Maxwell-Bloch equations. The role of non-Gaussian laser pulse shapes and the different cladding layers of the samples is analyzed. The measured radiative lifetime of 2D excitons is strongly influenced by reflective coupling between the quantum well and the air/sample interface. Depending on the thickness of the upper cladding layer the radiative dephasing time can be either increased or decreased as compared to the  $T_2$  of the bare quantum well. The effects of radiative coupling in a MQW Bragg structure can be significantly enhanced if the top layer is chosen as a  $\lambda/2$  layer (constructive superposition of surface reflected signal).

#### ACKNOWLEDGMENTS

Partial funding of this work through the Deutsche Forschungsgemeinschaft (Sonderforschungsbereich 383, the Leibniz prize), and a grant of CPU time on the T3E at the HLRZ Jülich is gratefully acknowledged.

#### APPENDIX: DERIVATION OF THE QUASISTATIONARY COUPLED EXCITON-PHOTON MODES

In the linear or quasistationary regime, Eqs. (4) can be solved in frequency space by inserting

$$P_n(\omega) = \chi(\omega)E(\omega, z_n) \quad (\text{A1})$$

for the polarization in the  $n$ th QW, where  $\chi(\omega)$  is the two-dimensional QW susceptibility, computed from the SBE. Inserting Eq. (A1) in Eqs. (4) and (5), one obtains for the total reflected field

$$E_R(z, \omega)e^{i\omega z/c_v} = -\frac{\sqrt{\epsilon}-1}{\sqrt{\epsilon}+1}E_0(\omega) + \frac{2\sqrt{\epsilon}}{\sqrt{\epsilon}+1}\frac{2\pi i\omega}{c\epsilon} \times \sum_{n,m=1}^N e^{i\omega z_n/c} \left( II - \frac{2\pi i\omega}{c\epsilon} \chi(\omega) \mathcal{D}(\omega) \right)_{n,m}^{-1} \times \chi(\omega)e^{i\omega z_m/c}E_0(\omega), \quad (\text{A2})$$

where  $II$  is the  $N \times N$  unit matrix and

$$\mathcal{D}(\omega) = \left( e^{i\omega|z_n-z_m|/c} + \frac{\sqrt{\epsilon}-1}{\sqrt{\epsilon}+1} e^{i\omega(z_n+z_m)/c} \right)_{n,m=1}^N. \quad (\text{A3})$$

In this regime, the solutions of the SMBE consist of coupled exciton-photon modes, having energies and radiative decay rates that are given by the poles of Eq. (A2). The poles depend on the positions  $z_n$  of the QW's and the number of coupled wells  $N$ . If the susceptibility exhibits a single strong resonance within the spectral range of the exciting laser pulse at  $\omega = \omega_0$ , we can approximate  $\exp(i\omega z_n/c) \approx \exp(i\omega_0 z_n/c)$  and  $\mathcal{D}(\omega) \approx \mathcal{D}(\omega_0)$ . Within this exciton-pole approximation, it can be shown that in the absence of the vacuum/semiconductor interface ( $\epsilon=1$ ), the observable quantities depend only on the phase  $\exp(2i\omega_0 d/c)$  accumulated while traveling back and forward from one QW to another.<sup>2</sup> Due to internal reflections at the cladding layers, the dynamics depends also on the absolute positions of the QW's, which can be recognized from Eq. (A3). In a perfect Bragg structure where  $d$  is equal to an integer multiple of half the heavy-hole exciton resonance wavelength  $\lambda_{hh} = 2\pi c/\omega_0$  inside the medium, on arrival, photons reemitted from the coherent polarization in a certain QW oscillate in phase with the polarization of any other QW. In these structures, a stimulated polarization decay due to reemitted photons is the dominating coupling mechanism between excitons in the different wells leading to an  $N$  times enhanced radiative dephasing rate. However, depending on the thickness of the first cladding layer, photons that have been reflected at the first interface can have a different phase, thus modifying the dynamics of the system. Mathematically, this can be seen from Eq. (A2) by diagonalizing the matrix  $\mathcal{D}(\omega_0)$ . For  $z_n = d_1 + (n-1)\lambda_{hh}/2$ , the vector  $1/\sqrt{N}((-1)^n)_{n=1}^N$  is an eigenvector of  $\mathcal{D}(\omega_0)$  with eigenvalue  $N(1+(\sqrt{\epsilon}-1)/(\sqrt{\epsilon}+1)\exp(2i\omega_0 d_1/c))$ . This eigenvector corresponds to the superradiant mode, while all other eigenvectors have the eigenvalue 0 and correspond to dark or subradiant modes. Only the superradiant mode contributes to the reflected signal:

$$\begin{aligned}
E_R(z, \omega) e^{i\omega_0 z/c_v} &= -\frac{\sqrt{\epsilon}-1}{\sqrt{\epsilon}+1} E_0(\omega) + e^{2i\omega_0 d_1/c} \frac{2\sqrt{\epsilon}}{\sqrt{\epsilon}+1} \frac{2\pi i \omega_0}{c\epsilon} \\
&\times \frac{N\chi(\omega)}{1 - \frac{2\pi i \omega_0}{c\epsilon} N\chi(\omega) \left(1 + \frac{\sqrt{\epsilon}-1}{\sqrt{\epsilon}+1} e^{2i\omega_0 d_1/c}\right)} E_0(\omega). \tag{A4}
\end{aligned}$$

From Eq. (A4) it can be recognized that, within the exciton-pole approximation, the reflection of a perfect Bragg structure differs from a SQW only by the replacement  $\chi \rightarrow N\chi$ , expressing the enhancement of the coupling between the semiconductor and the optical field. According to theoretical predictions,<sup>2,3</sup> the radiative coupling strength of the superradiant mode strongly decreases if  $d$  is slightly detuned from the Bragg condition. If the mismatch between  $d$  and  $\lambda_{\text{hh}}$  is increased, a rapidly growing part of the oscillator strength is transferred from the superradiant mode to the  $N-1$  optically dark modes, which have for small deviations between  $\lambda_{\text{hh}}$  and  $d$  even smaller radiative coupling strengths than in the corresponding SQW. To investigate the limitations of the exciton-pole approximation, we insert

$$\chi(\omega) = -\frac{|\sum_{\mathbf{k}} \mu_{\mathbf{k}} \varphi(\mathbf{k})|^2}{\omega - \omega_0 + i\gamma_0} \tag{A5}$$

for the linear two-dimensional  $1s$  exciton, yielding

$$\begin{aligned}
E_R(z, \omega) e^{i\omega_0 z/c_v} &= -\frac{\sqrt{\epsilon}-1}{\sqrt{\epsilon}+1} E_0(\omega) - e^{2i\omega_0 d_1/c} \frac{2\sqrt{\epsilon}}{\sqrt{\epsilon}+1} \\
&\times \frac{iN\Gamma}{\omega - \omega_0 - N\Delta\omega_{\text{rad}} + i\gamma_0 + iN\Gamma_s} E_0(\omega), \tag{A6}
\end{aligned}$$

where we defined

$$\Gamma = \frac{2\pi\omega_0}{c\epsilon} \left| \sum_{\mathbf{k}} \mu_{\mathbf{k}} \varphi(\mathbf{k}) \right|^2 = \frac{4\pi^2}{\epsilon\lambda_{\text{hh}}} \left| \sum_{\mathbf{k}} \mu_{\mathbf{k}} \varphi(\mathbf{k}) \right|^2 \tag{A7}$$

as the radiative dephasing rate of a SQW in the absence of the cladding layers, and

$$\Gamma_s = \Gamma \left( 1 + \frac{\sqrt{\epsilon}-1}{\sqrt{\epsilon}+1} \cos(4\pi d_1/\lambda_{\text{hh}}) \right), \tag{A8}$$

$$\Delta\omega_{\text{rad}} = \Gamma \frac{\sqrt{\epsilon}-1}{\sqrt{\epsilon}+1} \sin(4\pi d_1/\lambda_{\text{hh}}) \tag{A9}$$

are the radiative decay rate and the radiative shift of the  $1s$  exciton of the SQW in the presence of a top layer of thickness  $d_1$ . From Eq. (A6) it can be recognized that, within the exciton-pole approximation, the radiative decay rate of a MQW Bragg structure increases linearly with the QW number. However, if the radiative width approaches the same order of magnitude as the exciton binding energy, radiative coupling of the  $1s$  exciton to the higher excitonic bound states and the continuum states can no longer be neglected and the single exciton-pole approximation fails. Numerical calculations indicate significant deviations from the exciton-pole approximation for  $N \gtrsim 30$ , where the coupling to the continuum states yields a clearly asymmetric line shape although the linewidth is still approximately proportional to the QW number. Only in the superlattice limit  $N \rightarrow \infty$  and the absence of surface effects, the radiative width of a periodic MQW vanishes and stationary polariton states with the dispersion relation

$$\cos(qd) = \cos(\omega d/c) + \frac{2\pi\omega}{c} \chi(\omega) \sin(\omega d/c) \tag{A10}$$

are recovered, where  $d$  is the period of the structure.<sup>1,16</sup>

<sup>1</sup>E. L. Ivchenko, A. I. Nesvizhskii, and S. Jorda, *Phys. Solid State* **36**, 1156 (1994).

<sup>2</sup>T. Stroucken, A. Knorr, P. Thomas, and S. W. Koch, *Phys. Rev. B* **53**, 2026 (1996).

<sup>3</sup>M. Hübner, J. Kuhl, T. Stroucken, A. Knorr, S. W. Koch, R. Hey, and K. Ploog, *Phys. Rev. Lett.* **76**, 4199 (1996).

<sup>4</sup>E. Hanamura, *Phys. Rev. B* **38**, 1228 (1988).

<sup>5</sup>L. C. Andreani, F. Tassone, and F. Bassani, *Solid State Commun.* **77**, 641 (1991).

<sup>6</sup>B. Deveaud, F. Clérot, N. Roy, K. Satzke, B. Sermage, and D. S. Katzer, *Phys. Rev. Lett.* **67**, 2355 (1991).

<sup>7</sup>A. Vinattieri, J. Shah, T. C. Damen, D. S. Kim, L. N. Pfeiffer, M. Z. Maialle, and L. J. Sham, *Phys. Rev. B* **50**, 10 868 (1994).

<sup>8</sup>H. Wang, Kyle Ferrio, D. G. Steel, Y. Z. Hu, R. Binder, and S. W. Koch, *Phys. Rev. Lett.* **71**, 1261 (1993).

<sup>9</sup>Y. Yamamoto, S. Machida, Y. Horikoshi, K. Igeta, and G. Björk, *Opt. Commun.* **80**, 337 (1991).

<sup>10</sup>N. Ochi, T. Shiotani, M. Yamanishi, Y. Honda, and I. Suemune, *Appl. Phys. Lett.* **58**, 2735 (1991).

<sup>11</sup>A. P. Heberle, J. J. Baumberg, and K. Köhler, *Phys. Rev. Lett.* **75**, 2598 (1995).

<sup>12</sup>See, e.g., Chapter 12 in H. Haug and S. W. Koch, *Quantum Theory of the Optical and Electronic Properties of Semiconductors*, 3rd ed. (World Scientific, Singapore, 1994).

<sup>13</sup>R. Binder and S. W. Koch, *Prog. Quantum Electron.* **19**, 307 (1995).

<sup>14</sup>F. Jahnke, Habilitation thesis, Philipps-Universität Marburg, 1996; F. Jahnke, M. Kira, and S. W. Koch, *Z. Phys. B* **104**, 559 (1997).

<sup>15</sup>The parameters used for the numerical calculation are  $m_e = 0.071m_0$ ,  $m_h = 0.25m_0$ , where  $m_0$  is the free-electron mass,  $\epsilon = 12.53$ ,  $\gamma_0^{-1} = 50$  ps, and  $\mu_{\mathbf{k}=0} = 6.75$  Å.

<sup>16</sup>L. C. Andreani, *Phys. Status Solidi B* **188**, 29 (1995).